Lifetime measurements in Ce I, Ce II, and Ce III using time-resolved laser spectroscopy with application to stellar abundance determinations of cerium

Z. S. Li,[1,*] H. Lundberg,[1] G. M. Wahlgren,[2] and C. M. Sikström[2]
[1]*Department of Physics, Lund Institute of Technology, P.O. Box 118 S-221 00 Lund, Sweden*
[2]*Atomic Spectroscopy, Department of Physics, University of Lund, P.O. Box 118 S-221 00 Lund, Sweden*
(Received 3 February 2000; published 14 August 2000)

Radiative lifetimes of two levels in Ce I, eight levels in Ce II, and nine levels in Ce III have been measured using the time-resolved laser-induced fluorescence technique. Free cerium atoms and singly and doubly ionized ions were obtained in a laser-produced plasma. A narrow bandwidth UV laser pulse was employed to selectively populate the short-lived upper levels and the lifetime values were evaluated from the time-resolved fluorescence signals recorded by a fast detection system. Transition probabilities for Ce III were obtained from branching fractions calculated by the Cowan code and the experimental lifetimes. The results are compared with previous measurements and calculations. Spectral lines of Ce III were identified in the spectrum of the magnetic chemically peculiar star α^2CVn and the abundance of cerium was determined from synthetic spectrum fitting to be 800 times greater than the solar abundance.

PACS number(s): 32.70.Cs, 42.62.Fi

I. INTRODUCTION

Accurate atomic data such as energy levels and oscillator strengths are needed in the analysis of solar and stellar spectra with regard to the understanding of nucleosynthesis and atmospheric processes. In the hot chemically peculiar stars, characterized by the effective temperature range $T_{\rm eff}$=8000 to 13 000 K, the doubly ionized ions are typically the dominant ionization stage for the lanthanide elements. However, the lines used for identification and abundance determination are usually from the second spectrum, the reason in part being the scarce availability of reliable atomic data for the third spectrum. This condition has motivated several theoretical studies, for example the recent publications on Er III [1], Ce III [2,3], and Nd III [4]. Experimental oscillator strengths are required to check the theoretical approaches, and they can be determined by combining measurements of the radiative lifetime with relative intensities of lines originating from a given energy level.

The most reliable lifetime measurements are performed with techniques employing a selective excitation of the level to be investigated, for example using a tunable laser. However, few experimental results for doubly ionized ions using such techniques are available in the literature. The reason lies in the existence of considerable practical difficulties. First, it is difficult to produce doubly charged ions in common beam sources like thermo-ovens or hollow cathodes. Second, the level lifetimes of the third spectrum are often very short (1 or 2 ns), which means that a fast excitation and detection system is needed to perform an accurate measurement. Third, using photoexcitation, the wavelengths often fall in the ultraviolet (UV) or vacuum-ultraviolet (VUV) regions.

At the Lund Laser Center VUV laboratory [5], we have recently greatly extended the possibilities for lifetime measurements with the time-resolved laser-induced fluorescence (LIF) method [6,7]. A laser-produced plasma is used as an efficient source of multicharged ions. Stimulated Brillouin scattering (SBS) is employed to compress the 8-ns laser pulses from a commercial laser system to 1 ns. Combined with a fast detection system, lifetimes as short as 1 ns can be readily measured with an uncertainty around 10%. The recently published lifetime measurements on La III [8] are believed to constitute the first lifetime results of doubly ionized lanthanide ions using selective laser excitation and a cascade-free detection method. Following that, the laser spectroscopic lifetime measurements on Lu III [9] and Eu III [10] were also performed. For the joint purpose of providing data for testing theoretical calculations as well as application to astrophysics, in particular for stellar elemental abundance analyses, systematic investigations on radiative lifetimes of doubly charged lanthanide elements are being undertaken.

Previously, only two cascade-free lifetime measurements of multicharged ions have been reported. With the beam-foil laser technique, Baudinet-Robinet *et al.* [11] measured the $2p3s\ ^1P^o$ lifetime in O III. Langhans *et al.* [12] reported the measurement of the $5p\ ^5P_3$ lifetime in Kr III using the time-resolved LIF method, in which doubly ionized krypton ions were prepared by an electron beam impacting the effusive beam from a hollow-cathode lamp.

In 1991 Bisson *et al.* [13] published a series of experimental oscillator strengths for Ce I. Data were obtained by combining the measured branching ratios with lifetime results measured by a delayed photoionization technique. Beam-foil lifetime results for four low-lying levels of Ce II were reported by Andersen *et al.* [14] in 1975. Langhans *et al.* [15] published lifetime results of 11 levels of Ce II using laser spectroscopic measurement in 1995. Beam-foil lifetime measurements of six levels in the $4f6p$ configuration of Ce III were reported by Andersen *et al.* [16] in 1974. Their lifetime results have been compared by Bord *et al.* [3] with their recent calculations. The divergence between the experimental and calculated values partly motivates the present work to check the beam-foil measurements, which were performed more than 25 years ago.

*Email address: Li.zhongshan@fysik.lth.se

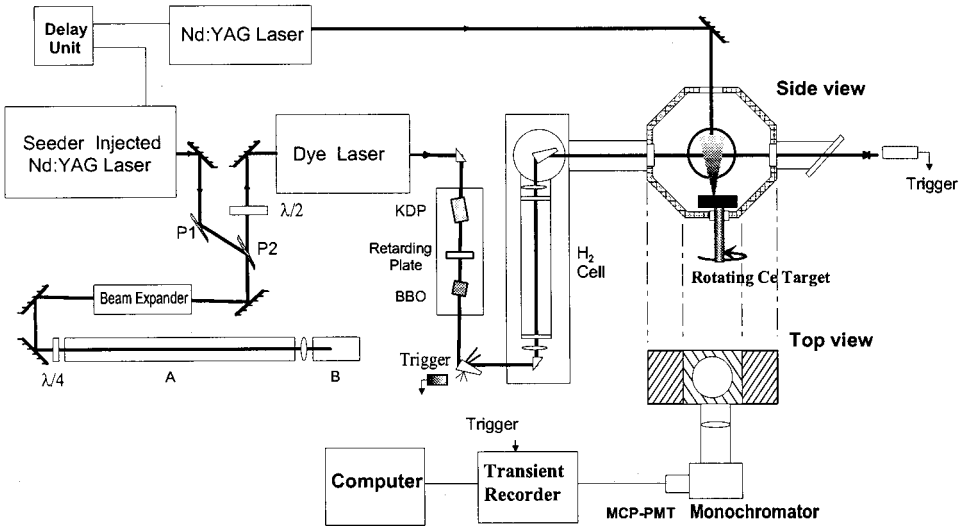

FIG. 1. Experimental setup.

In the present work, natural lifetimes were measured by time-resolved observation of laser-induced fluorescence. Free Ce, Ce^{+}, and Ce^{++} particles were obtained in a laser-produced plasma. Lifetimes have been measured for eight levels of singly ionized cerium, for which the transitions to lower levels constitute detectable lines in the solar spectrum. Lifetimes of nine levels of doubly ionized cerium have also been measured which, in addition to the interest to astrophysics, provide an effective check on the theoretical calculations from which larger amounts of data may be produced.

II. EXPERIMENTAL SETUP

The experimental setup is shown in Fig. 1. The 532-nm beam of 8-ns pulses from a seeder injected Nd:YAG (yttrium aluminum garnet) laser (Continuum NY-82) was compressed to 1 ns with a SBS compressor (a detailed description of this technique can be found in Ref. [6]). A dye laser (Continuum Nd-60) operated on DCM dye was pumped with this beam. The output from the dye laser is tunable from 615 to 660 nm, with a pulse energy of 10–20 mJ and a pulse duration of about 1 ns. To obtain the tunable UV radiation (210–450 nm), different nonlinear processes have been adopted. The second harmonic (2ω) was produced by frequency doubling in KDP; the third harmonic (3ω) was produced by frequency mixing of the second harmonic with the fundamental frequency in BBO. The Stoke (S) and anti-Stoke components (AS) of Raman shifting were generated in a H_2 gas cell. The schemes employed for the different levels are indicated in Table I.

A separate Nd:YAG laser (Continuum Surelite), which provided 532 nm, 10-ns pulses of roughly 5-mJ pulse energy, was used to perform ablation. This laser beam was focused perpendicularly onto a rotating metallic cerium target in the vacuum chamber. Free cerium atoms and singly and doubly charged ions were produced in the laser-induced plasma. The excitation laser beam was directed through the plasma about 5–10 mm above the ablation spot. Synchronization of all Nd:YAG lasers was achieved by external triggering from Standford Research Systems model 535 digital delay generator, which enabled a free variation of the delay time between the ablation pulse and the excitation pulse.

Laser-induced fluorescence from the selected upper levels was collected by a fused-silica lens, appropriately filtered by a $\frac{1}{8}$-m monochromator (resolution 6.4-nm/mm), and finally detected by a Hamamatsu 1564U microchannel-plate (MCP) photomultiplier tube (200-ps rise time). The data acquisition was performed by a digital transient recorder (Tektronix Model No. DSA 602) which has a 1-GHz bandwidth and was working either in real-time with a 2 GSamples/s sampling rate or in interleaved triggering with 5 GSamples/s sampling rate depending on the measured lifetime values. The averaged time-resolved fluorescence decay curves were transferred to a personal computer and lifetime evaluations were performed immediately in connection with the experiments.

III. MEASUREMENTS AND RESULTS

With appropriately chosen plasma conditions, free Ce^{+} and Ce^{++} ions and also Ce atoms with sufficient populations in different metastable states can be obtained. This enabled us to select favorable channels to populate the designated upper levels. To ensure that the correct level was excited, all strong decay channels were checked by tuning the monochromator, and then the strongest transition was selected for recording the decay curve (see Table I).

The plasma density and temperature at the observed spot can be adjusted by changing the ablation pulse energy, the size of the focus point, the distance above the target surface, and the delay time between the ablation and excitation pulses. To check the collisional quenching and radiation trapping effects, measurements under different plasma conditions were performed. For the measurements of the Ce I levels, the delay time between the ablation beam and the excitation beam could be as long as 12 μs with sufficient signal-to-noise ratio. The measured lifetimes in the delay time interval between 1.5 and 12 μs remained constant within the experimental scattering, while the detected fluorescence intensity varied by a factor of 15. The lifetimes of the Ce II levels are shorter than those of the Ce I, so it is reasonable to believe that the collisional quenching effects are relatively small in similar environments. As a test, the

TABLE I. Levels measured and excitation schemes.

Level[a]	E_{exp} (cm^{-1})	Excitation Origin	Excitation λ $(nm)_{vac.}$	Exc. laser wavelength conversion scheme	Observed fluorescence $(nm)_{vac.}$
Ce I					
$J=3$	22 600.482	0	442.47	$2\omega+2S$	469.0
$J=2$	22 970.284	228.849	439.73	$2\omega+2S$	485.4
Ce II					
$4f5d(^1G^o)6p\ J=9/2$	24 663.053	1873.934	438.81	$2\omega+2S$	422.4
$4f5d(^1G^o)6p\ J=72$	25 945.369	0	332.22	2ω	429.1
$4f5d(^3H^o)6p^2I_{13/2}$	34 513.468	2879.695	316.12	2ω	390.8
$4f5d(^3H^o)6p^2I_{11/2}$	32 802.165	987.611	314.32	2ω	398.6
$4f5d(^3P^o)6p\ J=7/2$	39 394.990	4523.033	286.76	$2\omega+AS$	347.8
$4f^2(^3H_4)6p_{1/2}(4,1/2)^o_{1/2}$	26 268.203	3854.012	446.15	$2\omega+2S$	452.4
$4f^2(^3H_4)6p_{1/2}(5,1/2)^o_{9/2}$	27 975.619	3854.012	414.57	$2\omega+2S$	447.2
$4f^2(^3H_4)6p_{1/2}(5,1/2)^o_{11/2}$	27 378.515	4165.550	430.79	$2\omega+2S$	457.4
Ce III					
$4f(^2F^o)6p(5/2,1/2)_2$	48 404.86	3821.53	224.23	$3\omega+S$	345.4
$4f(^2F^o)6p(5/2,1/2)_3$	48 267.00	3276.66	222.20	3ω	347.1
$4f(^2F^o)6p(5/2,3/2)_2$	51 640.68	6571.36	221.81	3ω	308.5
$4f(^2F^o)6p(5/2,3/2)_3$	51 262.21	5127.27	216.69	3ω	314.4
$4f(^2F^o)6p(5/2,3/2)_4$	52 440.96	6361.27	217.02	3ω	303.2
$4f(^2F^o)6p(7/2,1/2)_3$	50 375.00	5127.27	220.94	3ω	345.9
$4f(^2F^o)6p(7/2,1/2)_4$	50 057.60	3276.66	213.70	3ω	354.5
$4f(^2F^o)6p(7/2,3/2)_3$	53 615.98	6571.36	215.14	3ω	311.3
$4f(^2F^o)6p(7/2,3/2)_4$	54 549.34	7150.05	210.91	3ω	305.7

[a]Level designations and energies are from NIST Atomic Spectroscopic Database [20].

lifetimes of the Ce II levels were measured under the same plasma conditions as for the Ce I levels. The delay time could then be varied between 1 and 3 μs with reasonably strong fluorescence signals. The detected intensity then varied by a factor of 10, but the evaluated lifetime values remained constant. This indicated that collisional quenching and radiative trapping effects were negligible under our measurement conditions. The lifetime values of the Ce III levels are even shorter, and the decay curves could be characterized with only a few fluorescence photons as the background from the plasma and the excitation laser was negligible. The measurements were performed under the same plasma condition as those for Ce I and Ce II levels, while the delay time could be varied only within 0.5–1.5 μs in order to keep a reasonably strong fluorescence signal. No systematic effects were observed for measurements with different delay times.

Possible flight-out-of-view effects were specially investigated by changing the monochromator slit width and position. The temporal shape of the excitation pulse was recorded with the same detection system by detecting the scattered light of the laser pulse from a metal rod, which was inserted into the interaction spot of the cerium ion beam and the excitation beam. The recorded curve is, in fact, the convolution of the real laser pulse and the time-response function of the detection system. By fitting the fluorescence signal to the convolution of the detected laser pulse and a pure exponential function, the effects of the finite duration of the excitation laser pulse and the limited response time of the detection system were taken into account. To ensure the precision of this convolutional fitting, saturation of the excitation was effectively prevented by inserting neutral-density filters in the excitation laser beam to reduce the power. A typical decay curve and the corresponding convolution fit are shown in Fig. 2. In order to check the electronic bandwidth limitations of the detection system, the well-known lifetime of the short-lived Be I $2s2p\ ^1P_1$ level was measured with the same experimental setup. Our result is 1.79(10) ns, which is

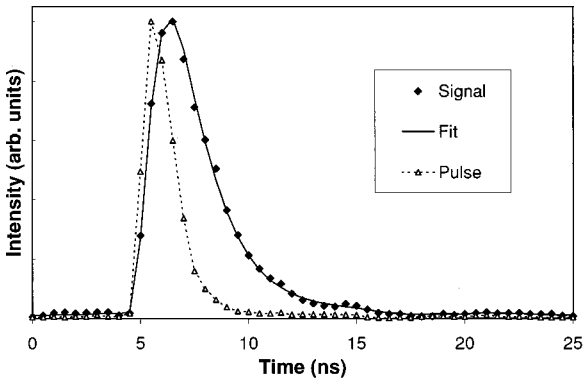

FIG. 2. Detected time-resolved fluorescence signal from the (Ce III) $4f\ (^2F^o)\ 6p(5/2,3/2)_3$ state and the recorded excitation laser pulse. The convolution procedure gives a lifetime of 1.55 ns.

TABLE II. Radiative lifetime measurements of Ce I, Ce II, and Ce III levels.

Level	Energy (cm^{-1})	Lifetime (ns) This work Expt.	This work Calc.	Previous Expt.	Previous Calc.
Ce I					
$J=3$	22 600.482	24(2)		26(3)[a]	
$J=2$	22 970.284	20(2)		23(3)[a]	
Ce II					
$4f5d(^1G^o)6p\ J=9/2$	24 663.053	7.0(4)		8.9(4)[b]	
$4f5d(^1G^o)6p\ J=7/2$	25 945.369	6.6(4)		10.9(5)[b]	
$4f5d(^3H^o)6p^2I_{13/2}$	34 513.468	4.7(4)			
$4f5d(^3H^o)6p^2I_{11/2}$	32 802.165	4.7(4)			
$4f5d(^3P^o)6p\ J=7/2$	39 394.990	2.6(3)			
$4f^2(^3H_4)6p_{1/2}(4,1/2)^o_{7/2}$	26 268.203	6.0(4)			
$4f^2(^3H_4)6p_{1/2}(5,1/2)^o_{9/2}$	27 975.619	6.1(4)		7.1(3)[b]	
$4f^2(^3H_4)6p_{1/2}(5,1/2)^o_{11/2}$	27 378.515	6.1(4)			
Ce III					
$4f(^2F^o)6p(5/2,1/2)_2$	48 404.86	2.00(20)	1.74	3.3(4)[c]	1.49[d]
$4f(^2F^o)6p(5/2,1/2)_3$	48 267.00	1.80(20)	1.50	3.3(5)[c]	1.45[d]
$4f(^2F^o)6p(5/2,3/2)_2$	51 640.68	1.70(20)	1.46		1.46[d]
$4f(^2F^o)6p(5/2,3/2)_3$	51 262.21	1.55(20)	1.25	3.7(5)[c]	1.25[d]
$4f(^2F^o)6p(5/2,3/2)_4$	52 440.96	1.60(20)	1.29	3.5(4)[c]	1.19[d]
$4f(^2F^o)6p(7/2,1/2)_3$	50 375.00	1.90(20)	1.57	3.2(4)[c]	1.48[d]
$4f(^2F^o)6p(7/2,1/2)_4$	50 057.60	4.2(4)	3.60	3.1(5)[c]	5.76[d]
$4f(^2F^o)6p(7/2,3/2)_3$	53 615.98	1.65(20)	1.40		1.51[d]
$4f(^2F^o)6p(7/2,3/2)_4$	54 549.34	1.60(20)	1.34		1.35[d]

[a]Bisson *et al.* (1991) [13] (laser spectroscopy).
[b]Langhans *et al.* (1995) [15] (time-resolved laser-induced fluorescence).
[c]Andersen *et al.* (1974) [16] (beam foil).
[d]Bord *et al.* (1997) [3] (HF calculation).

in good agreement with the previous theoretical [17] and experimental value [18].

To ensure a linear response of the detection system, only a few fluorescence photons were detected for each pulse in the measurements. An average of 1000–4000 pulses was necessary for each curve depending on the signal-to-noise ratio. Around 30 curves for each level have been recorded and the averaged lifetime value was adopted as the final result. The quoted error bar of the reported lifetimes is a conservative estimation of the combined random and systematic error, while the standard deviations of different measurements are less than 50% of the quoted uncertainties. The experimental lifetime results are given in Table II.

IV. THEORETICAL CALCULATION

Theoretical transition probabilities (A values) of Ce III were calculated in order to derive branching fractions (BF's). This was done using the Cowan computer code [19]. The set of programs were run in Hartree-Fock mode, including relativistic effects. The even configurations $4f^2$,$4f6p$,$4f7p$, $4f5f$,$4f6f$,$4f7f$,$5d6s$,$5d7s$,$5d^2$,$5d6d$,$6s^2$,$6p^2$ and the odd configurations $4f5d$,$4f6d$,$4f7d$,$4f6s$,$4f7s$,$4f8s$,$4f5g$, $4f6g$,$5d6p$,$6s6p$ were included in our calculation. Similar calculations of Ce III, also using the Cowan code, have been presented by Bord *et al.* [3] and Wyart and Palmeri [2]. For the even configurations $4f^2$, $5d^2$, $4f6p$, and $5d6s$, the parameters published by Wyart and Palmeri [2] were used. For all other configurations, the Hartree-Fock (HF) parameters were scaled to 80% of their original values. This scaling factor was determined by comparing the fitted parameters by Wyart and Palmeri [2] to the unscaled HF parameters for all levels for which parameters were published. This was also necessary for the two odd configurations $4f5d$ and $4f6s$, which consist of the lower levels of the transitions published in this paper, because no parameters are given in paper [2].

Special attention should be paid to the even levels in the $4f6p$ configuration with $J=4$. These levels are strongly mixed with the level $5d^2\ ^1G_4$. This level is not identified by name in the compilation by Martin *et al.* [20], but is expected to appear inside the $4f6p$ configuration. Both the calculation and the experimental lifetime indicate that the level at 50 057.60 cm^{-1} termed $4f6p(7/2,1/2)_4$ in the compilation by Martin *et al.* [20] would be more appropriately named as $5d^2\ ^1G_4$. Also, the level at 50 057.60 cm^{-1} is

TABLE III. Transition probabilities of Ce III. gA_{scaled} = scaled gA_{theory} values using the experimental lifetimes in Table II. $gA_{theory} = gA$ values calculated using the Cowan computer code [19]. $gA_{W\&P} = gA$ values published by Wyart and Palmeri [2].

Upper-level energy (cm^{-1})	J	Lower-level energy (cm^{-1})	J	σ (cm^{-1})	λ_{air} (Å)	gA_{scaled}	gA_{theory}	$gA_{W\&P}$	log gf
48 267.00	3	3276.66	4	44 990.34	2222.008	1.12 [+09]	1.35 [+09]	1.57 [+09]	−0.08
		3821.53	2	44 445.47	2249.251	1.38 [+08]	1.66 [+08]		−0.98
		5127.27	4	43 139.73	2317.337	4.30 [+08]	5.17 [+08]	3.55 [+08]	−0.46
		5502.37	3	42 764.63	2337.664	9.27 [+07]	1.12 [+08]		−1.12
		6265.21	3	42 001.79	2380.125	5.03 [+08]	6.05 [+08]	5.38 [+08]	−0.37
		6571.36	2	41 695.64	2397.602	6.59 [+07]	7.93 [+07]		−1.25
		7150.05	4	41 116.95	2431.349	4.75 [+06]	5.71 [+06]		−2.38
		7836.72	4	40 430.28	2472.646	3.24 [+07]	3.89 [+07]		−1.53
		9900.49	2	38 366.51	2605.661	2.21 [+06]	2.66 [+06]		−2.65
		10 126.53	3	38 140.47	2621.105	1.03 [+08]	1.24 [+08]		−0.97
		12 500.72	3	35 766.28	2795.105	1.76 [+07]	2.12 [+07]		−1.69
		12 561.55	2	35 625.45	2806.155	3.46 [+06]	4.16 [+06]		−2.39
		19 236.23	2	29 030.77	3443.634	5.30 [+08]	6.37 [+08]	6.37 [+08]	−0.03
		19 464.46	3	28 802.54	3470.922	8.04 [+08]	9.67 [+08]	9.78 [+08]	0.16
		21 849.47	3	26 417.53	3784.290	4.23 [+07]	5.09 [+07]	4.54 [+07]	−1.04
48 404.86	2	3821.53	2	44 583.33	2242.295	6.54 [+08]	7.51 [+08]	8.90 [+08]	−0.31
		5502.37	3	42 902.49	233.152	6.17 [+06]	7.09 [+06]		−2.30
		6265.21	3	42 139.65	2372.338	5.73 [+08]	6.59 [+08]	7.30 [+08]	−0.32
		6571.36	2	41 833.50	2389.700	9.27 [+07]	1.07 [+08]		−1.10
		8922.05	1	39 482.81	2531.987	2.32 [+08]	2.67 [+08]	2.95 [+08]	−0.65
		9900.49	2	38 504.37	2596.332	3.88 [+06]	4.46 [+06]		−2.41
		10 126.53	3	38 278.33	2611.664	7.70 [+06]	8.85 [+06]		−2.10
		11 612.67	1	36 792.19	2717.163	2.85 [+07]	3.28 [+07]		−1.50
		12 500.72	3	35 904.14	2784.373	6.66 [+05]	7.65 [+05]		−3.11
		12 641.55	2	35 763.31	2795.338	2.48 [+07]	2.85 [+07]		−1.54
		18 443.63	1	29 961.23	3336.687	1.48 [+07]	1.70 [+07]	1.53 [+07]	−1.61
		19 236.23	2	29 168.63	3427.358	3.55 [+08]	4.08 [+08]	4.84 [+08]	−0.20
		19 464.46	3	28 940.40	3454.388	5.06 [+08]	5.81 [+08]	6.06 [+08]	−0.04
		21 849.47	3	26 555.39	3764.644	8.09 [+05]	9.30 [+05]		−2.76
50 375.00	3	3276.66	4	47 098.34	2122.546	1.17 [+08]	1.41 [+08]		−1.10
		3821.53	2	46 553.47	2147.392	3.25 [+07]	3.93 [+07]		−1.65
		5127.27	4	45 247.73	2209.367	7.50 [+07]	9.06 [+07]	1.19 [+08]	−1.26
		5502.37	3	44 872.63	2227.837	5.77 [+08]	6.97 [+08]	7.18 [+08]	−0.37
		6265.21	3	44 109.79	2266.369	1.04 [+07]	1.25 [+07]		−2.10
		6571.36	2	43 803.64	2282.211	3.94 [+07]	4.76 [+07]		−1.51
		7150.05	4	43 224.95	2312.768	2.35 [+07]	2.84 [+07]		−1.72
		7836.72	4	42 538.28	2350.104	6.16 [+08]	7.44 [+08]	7.67 [+08]	−0.29
		9900.49	2	40 474.51	2469.944	3.79 [+08]	4.58 [+08]	4.74 [+08]	−0.46
		10 126.53	3	40 248.47	2483.817	3.43 [+08]	4.15 [+08]	3.41 [+08]	−0.50
		12 500.72	3	37 874.28	2639.528	3.73 [+05]	4.50 [+05]		−3.41
		12 641.55	2	37 733.45	2649.380	1.65 [+08]	1.99 [+08]		−0.76
		19 236.23	2	31 138.77	3210.503	1.42 [+07]	1.72 [+07]	2.06 [+07]	−1.66
		19 464.46	3	30 910.54	3234.209	8.19 [+07]	9.90 [+07]	1.09 [+08]	−0.89
		21 476.46	4	28 898.54	3459.392	7.47 [+08]	9.03 [+08]	8.34 [+08]	0.13
		21 849.47	3	28 525.53	3504.629	4.64 [+08]	5.61 [+08]	6.29 [+08]	−0.07

given $5d^2\ ^1G_4$ as the leading percentage from the Cowan code. However, the leading percentage for the $J=4$ levels in the $4f6p$ configuration is about 50% in our calculation. The transition probabilities of lines involving these levels should be expected to be more uncertain, since the mixing between levels is sensitive to the energy difference between the $J=4$ levels.

Both our experimental and theoretical lifetimes derived

TABLE III. (*Continued*).

Upper-level energy (cm^{-1})	J	Lower-level energy (cm^{-1})	J	σ (cm^{-1})	λ_{air} (Å)	gA_{scaled}	gA_{theory}	$gA_{W\&P}$	log gf
51 262.21	3	3276.66	4	47 985.55	2083.297	7.58 [+07]	9.37 [+07]		−1.31
		3821.53	2	47 440.68	2107.228	9.24 [+06]	1.14 [+07]		−2.21
		5127.27	4	46 134.94	2166.875	1.35 [+09]	1.67 [+09]	1.82 [+09]	−0.02
		5502.37	3	45 759.84	2184.639	3.08 [+08]	3.81 [+08]		−0.66
		6265.21	3	44 997.00	2221.679	5.96 [+07]	7.37 [+07]		−1.35
		6571.36	2	44 690.85	2236.900	1.22 [+08]	1.51 [+08]		−1.04
		7150.05	4	44 112.16	2266.248	4.63 [+05]	5.73 [+05]		−3.45
		7836.72	4	43 425.49	2302.086	4.62 [+08]	5.72 [+08]	4.91 [+08]	−0.43
		9900.49	2	41 361.72	2416.960	1.47 [+07]	1.82 [+07]	2.00 [+07]	−1.89
		10 126.53	3	41 135.68	2430.242	3.01 [+08]	3.72 [+08]	3.05 [+08]	−0.57
		12 500.72	3	38 761.49	2579.108	1.01 [+07]	1.25 [+07]		−2.00
		12 641.55	2	38 620.66	2588.513	2.51 [+07]	3.11 [+07]		−1.60
		19 236.23	2	32 025.98	3121.560	1.09 [+09]	1.35 [+09]	1.38 [+09]	0.20
		19 464.46	3	31 797.75	3143.966	6.05 [+08]	7.48 [+08]	7.16 [+08]	−0.05
		21 476.46	4	29 785.75	3356.346	9.73 [+06]	1.20 [+07]		−1.78
		21 849.47	3	29 412.74	3398.912	6.64 [+07]	8.21 [+07]	9.90 [+07]	−0.94
51 640.68	2	3821.53	2	47 819.15	2090.548	3.74 [+07]	4.36 [+07]		−1.61
		5502.37	3	46 138.31	2166.716	3.68 [+08]	4.30 [+08]		−0.59
		6265.21	3	45 375.47	2203.146	3.44 [+08]	4.01 [+08]		−0.60
		6571.36	2	45 069.32	2218.114	3.96 [+08]	4.62 [+08]	5.06 [+08]	−0.53
		8922.05	1	42 718.63	2340.182	1.40 [+06]	1.64 [+06]		−2.94
		9900.49	2	41 740.19	2395.043	1.90 [+08]	2.21 [+08]	2.56 [+08]	−0.79
		10 126.53	3	41 514.15	2408.085	1.38 [+08]	1.61 [+08]	1.72 [+08]	−0.92
		11 612.67	1	40 028.01	2497.498	2.51 [+08]	2.93 [+08]	3.03 [+08]	−0.63
		12 500.72	3	39 139.96	2554.167	4.12 [+06]	4.81 [+06]		−2.39
		12 641.55	2	38 999.13	2563.391	3.16 [+07]	3.68 [+07]		−1.51
		18 443.63	1	33 197.05	3011.438	1.24 [+07]	1.44 [+07]	2.03 [+07]	−1.77
		19 236.23	2	32 404.45	3085.100	7.92 [+08]	9.23 [+08]	9.12 [+08]	0.05
		19 464.46	3	32 176.22	3106.984	3.72 [+08]	4.34 [+08]	5.32 [+08]	−0.27
		21 849.47	3	29 791.21	3355.730	2.99 [+06]	3.48 [+06]		−2.30
52 440.96	4	3276.66	4	49 164.30	2033.342	2.01 [+08]	2.50 [+08]	2.64 [+08]	−0.90
		5127.27	4	47 313.69	2112.884	1.58 [+06]	1.96 [+06]		−2.98
		5502.37	3	46 938.59	2129.771	7.46 [+05]	9.28 [+05]		−3.29
		6265.21	3	46 175.75	2164.959	2.53 [+07]	3.14 [+07]		−1.75
		6361.27	5	46 079.69	2169.473	1.19 [+09]	1.49 [+09]	1.46 [+09]	−0.07
		7150.05	4	45 290.91	2207.260	5.01 [+08]	6.23 [+08]	4.65 [+08]	−0.44
		7836.72	4	44 604.24	2241.244	1.72 [+08]	2.14 [+08]		−0.89
		9325.51	5	43 115.45	2318.642	9.43 [+08]	1.17 [+09]	1.20 [+09]	−0.12
		10 126.53	3	42 314.43	2362.538	1.31 [+08]	1.63 [+08]		−0.96
		12 500.72	3	39 940.24	2502.986	3.76 [+07]	4.67 [+07]		−1.45
		16 152.32	5	36 288.64	2754.869	2.38 [+08]	2.95 [+08]	2.76 [+08]	−0.57
		19 464.46	3	32 976.50	3031.580	1.65 [+09]	2.05 [+09]	2.09 [+09]	0.36
		21 476.46	4	30 964.50	3228.573	4.35 [+08]	5.41 [+08]	5.27 [+08]	−0.17
		21 849.47	3	30 591.49	3267.941	9.25 [+07]	1.15 [+08]	1.16 [+08]	−0.83

with the Cowan code are given in Table III. A difference between the experimental and theoretical data is found, with the theoretical lifetimes being systematically lower. This is probably due to the neglected effect of core polarization (CP) in our calculation. Including CP in the calculation would tend to increase the calculated lifetimes, because the difference in the polarization of the core between the upper and lower level will make the transition probability lower. However, the effect can be expected to be larger on the sum of the transition probability than on the BR.

The *A* values calculated with the Cowan code were used to derive branching fractions, which were subsequently

TABLE III. (*Continued*).

Upper-level energy (cm^{-1})	J	Lower-level energy (cm^{-1})	J	σ (cm^{-1})	λ_{air} (Å)	gA_{scaled}	gA_{theory}	$gA_{W\&P}$	log gf
53 615.98	3	3276.66	4	50 339.32	1986.519	1.27 [+08]	1.50 [+08]		−1.12
		3821.53	2	49 794.45	2007.607	7.36 [+05]	8.68 [+05]		−3.35
		5127.27	4	48 488.71	2061.677	8.32 [+07]	9.80 [+07]		−1.28
		5502.37	3	48 113.61	2077.752	1.95 [+07]	2.30 [+07]		−1.90
		6265.21	3	47 350.77	2111.229	1.42 [+07]	1.67 [+07]		−2.02
		6571.36	2	47 044.62	2124.970	6.83 [+07]	8.04 [+07]		−1.33
		7150.05	4	46 465.93	2151.438	6.77 [+08]	7.98 [+08]	6.99 [+08]	−0.33
		7836.72	4	45 779.26	2183.712	2.46 [+08]	2.90 [+08]		−0.75
		9900.49	2	43 715.49	2286.813	9.54 [+05]	1.12 [+06]		−3.13
		10 126.53	3	43 489.45	2298.700	1.51 [+07]	1.78 [+07]		−1.92
		12 500.72	3	41 115.26	2431.449	8.38 [+08]	9.88 [+08]	7.88 [+08]	−0.13
		12 641.55	2	40 974.43	2439.807	4.63 [+08]	5.46 [+08]	6.18 [+08]	−0.38
		19 236.23	2	34 379.75	2907.837	4.58 [+05]	5.40 [+05]		−3.24
		19 464.46	3	34 151.52	2927.271	4.59 [+07]	5.41 [+07]		−1.23
		21 476.46	4	32 139.52	3110.532	5.37 [+08]	6.32 [+08]	7.80 [+08]	−0.11
		21 849.47	3	31 766.51	3147.058	1.11 [+09]	1.30 [+09]	1.15 [+09]	−0.22
54 549.34	4	3276.66	4	51 272.68	1950.356	2.04 [+08]	2.43 [+08]	2.18 [+08]	−0.93
		5127.27	4	49 422.07	2022.735	1.53 [+07]	1.82 [+07]	3.57 [+08]	−2.03
		5502.37	3	49 046.97	2038.207	2.37 [+07]	2.82 [+07]		−1.83
		6265.21	3	48 284.13	2070.413	3.16 [+06]	3.77 [+06]		−2.69
		6361.27	5	48 188.07	2074.541	7.05 [+06]	8.40 [+08]		−2.34
		7150.05	4	47 399.29	2109.068	5.33 [+08]	6.35 [+08]	6.02 [+08]	−0.45
		7836.72	4	46 712.62	2140.075	1.92 [+05]	2.29 [+05]		−3.88
		9325.51	5	45 223.83	2210.535	2.65 [+08]	3.16 [+08]		−0.71
		10 126.53	3	44 422.81	2250.398	1.65 [+05]	1.96 [+05]		−3.90
		12 500.72	3	42 048.62	2377.474	1.91 [+08]	2.28 [+08]	2.08 [+08]	−0.79
		16 152.32	5	38 397.02	2603.591	2.18 [+09]	2.59 [+09]	2.46 [+09]	0.34
		19 464.46	3	35 084.88	2849.393	2.19 [+08]	2.61 [+08]	2.96 [+08]	−0.57
		21 476.46	4	33 072.88	3022.745	4.79 [+08]	5.70 [+08]	5.79 [+08]	−0.18
		21 849.47	3	32 699.87	3057.227	1.51 [+09]	1.80 [+09]	1.79 [+09]	0.33
50 057.60	4	3276.66	4	46 780.94	2136.949	6.35 [+08]	7.37 [+08]	6.67 [+08]	−0.36
		5127.27	4	44 930.33	2224.976	1.62 [+08]	1.88 [+08]		−0.92
		5502.37	3	44 555.23	2243.709	1.78 [+07]	2.07 [+07]		−1.87
		6361.27	5	43 696.33	2287.816	8.88 [+07]	1.03 [+08]		−1.16
		7150.05	4	42 907.55	2329.877	4.03 [+06]	4.68 [+06]		−2.48
		7836.72	4	42 220.88	2367.773	1.11 [+08]	1.29 [+08]		−1.03
		9325.51	5	40 732.09	2454.324	2.22 [+08]	2.58 [+08]	2.47 [+08]	−0.70
		10 126.53	3	39 931.07	2503.561	5.25 [+07]	6.10 [+07]	6.36 [+07]	−1.31
		12 500.72	3	37 556.88	2661.836	5.98 [+06]	6.94 [+06]		−2.20
		16 152.32	5	33 905.28	2948.531	1.02 [+07]	1.18 [+07]	5.21 [+06]	−1.88
		19 464.46	3	30 593.14	3267.765	9.96 [+07]	1.16 [+08]	1.24 [+08]	−0.80
		21 476.46	4	28 581.14	3497.810	2.41 [+08]	2.80 [+08]	2.67 [+08]	−0.35
		21 849.47	3	28 208.13	3544.065	4.93 [+08]	5.72 [+08]	5.31 [+08]	−0.03

scaled using the experimental radiative lifetime results obtain in this work. All transitions with a scaled $\log_{10} gf > -4.0$ are given in Table III. Both the scaled (gA_{scaled}) and the unscaled (gA_{theory}) A values are given. Also, the A values ($gA_{W\&P}$) of Wyart and Palmeri [2] are given for comparison. The systematic difference between our scaled f values and those calculated by Wyart and Palmeri is due to a difference in their calculated and our measured lifetimes. A comparison between our calculated f values before scaling with experimental lifetimes and the values calculated by Wyart and Palmeri show an agreement within 15% for the stronger lines and within 30% for most of the other lines. The exception is the line at 2022.735 Å, which shows a difference in the calculated gA of almost a factor of 20. The cancellation factor

TABLE IV. Cerium abundance in $\alpha^2 CVn$ from the lines of Ce III.

λ (nm)	$\log N_{Ce}$
342.7358	3.9
344.3634	4.1
345.4388	4.1
345.9392	3.8
347.0922	3.8
350.4629	3.5

(CF) given by the Cowan program, which is often taken as a guide to the uncertainty in the *gA* value, did not suggest a larger uncertainty. Also, other lines from the upper level or to the lower level of the transition at 2022.735 Å did not show larger deviations between our calculation and that of Wyart and Palmeri. Therefore, no explanation for the discrepancy can be given at this time.

The air wavelengths given in Table III are calculated using the formula of Edlén [21] and the energy levels listed in Martin *et al.* [20]. The uncertainty of our scaled values in Table III is estimated to be no more than 50% for strong lines ($\log_{10} gf > 0$), while the weaker lines are more uncertain and may have larger errors attached to them. This estimate is based on comparisons between other Cowan code calculations of similar species and experimental data.

V. CERIUM ABUNDANCE IN α^2CVn

The decay lifetimes for the low excitation states of Ce^{++} described earlier correspond to intrinsically strong transitions, and for the temperatures found in the photospheres of chemically peculiar stars these transitions are detectable in sufficiently high resolution spectra. We apply our derived oscillator strengths for several of the strongest transitions of Ce^{++} to the identification of Ce III lines (see Table IV) in the spectrum of the magnetic chemically peculiar star α^2CVn (=HD112413, spectral type A0p). We then determine the cerium abundance at a particular stellar rotational phase by comparing the observed stellar spectrum with computed spectra.

α^2CVn is the prototype for the class of low-amplitude light and spectrum-variable stars that bears its name. The standard model for these observed variations involves an oblique rotator where the magnetic poles are not aligned along the rotation axis [22]. The spectrum and light variations are therefore modulated over the 5.469 39 day rotation period [23] by the chemical and thermal inhomogeneities of the stellar surface. The visual region of the spectrum of α^2CVn is replete with lines from the lanthanide elements, and its ultraviolet spectrum is a confusing blend of lines. Many ultraviolet spectral features remain unidentified, although many of these are suspected to arise from the lanthanide elements. Lines from the Ce II and Ce III spectra have been identified in this star [24]. From Ce II lines the abundance of cerium has been estimated to be 4.2 orders of magnitude greater than the solar value [25]. However, due to Ce^+ being a minority ionization state and subsequent improvements in model atmospheres and atomic data, caution should be exercised when interpreting this older cerium abundance.

As can be seen from Table III, the strongest lines of Ce III involving the low-excitation term occur in the region between 310 and 350 nm, a region typically ignored by ground-based observation. Spectra were obtained using the SOFIN echelle spectrograph [26] at the 2.5-m Nordic Optical Telescope, located at the Observatorio de Grand Canaries, La Palma, Spain, for the purpose of studying the spectral region 330 to 400 nm. The spectrum obtained on Julian Date JD2450913.525 occurred at phase 0.92 of the light curve. Phase 0.0 corresponds to the maximum observed strength for optical region Eu II lines and a minimum (maximum negative polarity) of the magnetic field strength. The spectral resolving power of the data is approximately $R = \lambda/\Delta\lambda = 75\,000$, and the signal-to-noise ratio of 60.

Synthetic spectra were generated using the SYNTHE program (Kurucz [27]) and an ATLAS9 model atmosphere defined by $T_{\rm eff} = 11\,500$ K, logarithmic gravity is 4.0, turbulent velocity is 1 km s^{-1}, and a metallicity enrichment of 0.5 dex [28]. The atomic line data for the SYNTHE program is that of Kurucz [27] with the exception of the Ce III data presented in this paper. The six strongest lines from Table III that are found in our observation window were all detected in the stellar spectrum and they alone are used for the cerium abundance analysis. An average of the best-fit abundances for these lines yields $\log_{10} N_{\rm Ce} = 4.4 +/- 0.2$ dex, which is 2.9 dex greater than the solar value, on a scale where the hydrogen abundance is given as $\log_{10} N_{\rm H} = 12.00$. The quoted error from the six lines does not represent a total error, which may also include the effects of unknowns such as the appropriateness of the model atmosphere and errors in atomic data for blended lines. The dominant source of line broadening is attributed to Doppler motion associated with the observed stellar rotation velocity of $v \sin i = 14$ km s^{-1} [28]. We have not included the line structure due to the magnetic field of the star since our work has not indicated a noticeable Zeeman broadening at these short wavelengths. At phase 0.0 the magnitude of the longitudinal magnetic field strength has been measured to be approximately 1 kGauss [29]. The influence of isotopic and hyperfine structure has also been neglected in our synthetic spectrum calculations. The isotopes of cerium are all even in atomic number and produce no net nuclear spin and therefore no hyperfine structure. The dominance of isotope ^{140}Ce by number (solar system composition: 88.48% ^{140}Ce, 11.07% ^{142}Ce, 0.25% ^{138}Ce, and 0.19% ^{136}Ce) in a highly line-blended spectrum, along with the unknown isotopic shifts for the energy levels of Ce III lines, precludes us from consideration of isotopic shift. Figure 3 presents the observed and computed spectral region which includes the Ce III lines at 3454.388 Å and 3459.392 Å.

VI. DISCUSSION

The lifetime data from the present investigation are compared with previously published experimental and theoretical results in Table II. The lifetime values for the two Ce I levels agree well within the quoted uncertainties with the laser ex-

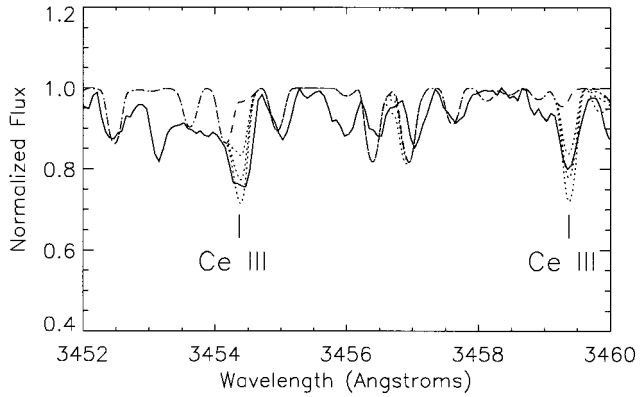

FIG. 3. Comparison of observed (solid line) and computed spectra for α^2CVn. The computed spectra represent cerium abundance at the levels of the solar abundance (dashed line), and 2.5, 3.0, and 3.5 dex enhancements (dotted lines).

citation and delayed photoionization measurement performed by Bisson *et al.* [13]. For the levels of Ce II, three of them have been measured in a previous time-resolved LIF experiment performed by Langhans *et al.* [15]. The previous values are found to be about 30% longer.

For the Ce III lifetimes, the discrepancies between the beam-foil measurement [16] and recent Hartree-Fock (HF) calculations [3] are substantial. The lifetime values presented in the current paper are closer to the calculation [3], though still systematically longer than the theoretical results. A similar condition occurs for the isoelectronic ion La II when comparing the laser spectroscopic measurements with HF calculations [8,30]. The most interesting case is the $J=4$ level at 50 057.60 cm^{-1}, which was measured to have a much longer lifetime than its neighboring levels. This can be explained by the fact that the level at 50 057.60 cm^{-1} should be renamed as $5d^2\ ^1G_4$, rather than belong to the $4d6p$ configuration.

Using oscillator strengths for the strong lines of Ce III derived from the experimental lifetimes and scaled theoretical branching ratios the abundance of cerium in the magnetic chemically peculiar star α^2CVn has been determined to be 2.9 dex greater than the solar value. The scatter in the abundance result is considered to originate primarily from issues of line blending and therefore reflects the goodness in the relative accuracy of the oscillator strengths.

ACKNOWLEDGMENTS

The authors would like to thank Dr. T. Brage and Dr. J.-O. Ekberg for guidance and valuable advice during the theoretical part of this work and I. Ilyin for help with the NOT data reduction. The support from Professor S. Svanberg is gratefully acknowledged. This work was financially supported by the Swedish Natural Science Research Council.

[1] J.-F. Wyart, J. Blaise, W. P. Bidelman, and C. R. Cowley, Phys. Scr. **56**, 446 (1997).
[2] J.-F. Wyart and P. Palmeri, Phys. Scr. **58**, 368 (1998).
[3] D. J. Bord, C. R. Cowley, and P. L. Norquist, Mon. Not. R. Astron. Soc. **284**, 869 (1997).
[4] C. R. Cowley and D. J. Bord, Astron. Soc. Pac. Conf. Ser. **143**, 346 (1998).
[5] S. Svanberg, J. Larsson, A. Persson, and C.-G. Wahlström, Phys. Scr. **49**, 187 (1994).
[6] Z. S. Li, J. Norin, A. Persson, C. G. Wahlström, S. Svanberg, P. S. Doidge, and E. Biémont, Phys. Rev. A **60**, 198 (1999).
[7] Z. S. Li, H. Lundberg, C. M. Sikström, and S. Johansson, Eur. Phys. J. D **6**, 9 (1999).
[8] Z. S. Li and Jiang Zhankui, Phys. Scr. **60**, 414 (1999).
[9] G. M. Wahlgren *et al.* (unpublished).
[10] Zhang Zhiguo, Z. S. Li, H. Lundberg, K. Zhang, Z. Dai, Jiang Zhankui, and S. Svanberg, J. Phys. B: At. Mol. Opt. **33**, 521 (2000).
[11] Y. Baudinet-Robinet, P. D. Dumont, and H. P. Garnir, Phys. Rev. A **43**, 4022 (1991).
[12] G. Langhans, W. Schade, and V. Helbig, Phys. Lett. A **183**, 205 (1993).
[13] C. E. Bisson, E. F. Worden, J. G. Conway, B. Comaskey, J. A. D. Stockdale, and F. Nehring, J. Opt. Soc. Am. B **8**, 1545 (1991).
[14] T. Andersen, O. Poulsen, P. S. Ramanujam, and A. P. Petkow, Sol. Phys. **44**, 257 (1975).
[15] G. Langhans, W. Schade, and V. Helbig, Z. Phys. D: At., Mol. Clusters **34**, 151 (1989).
[16] T. Andersen and G. Sørensen, Sol. Phys. **38**, 343 (1974).
[17] A. W. Weiss, Phys. Rev. A **51**, 1067 (1995).
[18] R. E. Irving, M. Henderson, L. J. Curtis, I. Martinson, and P. Bengtsson, Can. J. Phys. **77**, 137 (1999).
[19] R. D. Cowan, *The Theory of Atomic Structure and Spectra* (University of California Press, Berkeley, 1981). The Cowan code is available at different web sites, e.g., http://plasma-gate.weizmann.ac.il.
[20] W. C. Martin, R. Zalubas, and L. Hagan, *1978 Atomic Energy Levels—The Rare Earth Elements* (NIST, Washington, D.C., 1978).
[21] B. Edlén, Metrologia **2**, 71 (1966).
[22] D. M. Pyper, Astrophys. J., Suppl. **18**, 347 (1969).
[23] G. Farnsworth, Astrophys. J. **76**, 313 (1932).
[24] O. Struve and P. Swings, Astrophys. J. **98**, 361 (1943).
[25] J. G. Cohen, Astrophys. J. **159**, 473 (1970).
[26] I. Tuommen, Nordic Optical Telescope News **5**, 15 (1992).
[27] R. L. Kurucz, http://cfaku5.harvard.edu.
[28] G. M. Wahlgren, Contrib. Astron. Obs. Skalnaté Pleso **27**, 368 (1998).
[29] E. Borra and J. D. Landstreet, Astrophys. J. **212**, 141 (1977).
[30] D. J. Bord, L. P. Barisciano, Jr., and C. R. Cowley, Mon. Not. R. Astron. Soc. **278**, 997 (1996).